High-Spatial-Resolution Medical-Imaging System Using a HARPICON Camera Coupled with a Fluorescent Screen

Keiji Umetani,[a] Hironori Ueki,[a] Ken Ueda,[a] Tadaaki Hirai,[a]† Tohoru Takeda,[b] Toshiki Doi,[b] Jin Wu,[b] Yuji Itai[b] and Masayoshi Akisada[c]

[a]Central Research Laboratory, Hitachi Ltd, Kokubunji, Tokyo 185, Japan, [b]Institute of Clinical Medicine, University of Tsukuba, Tsukuba, Ibaraki 305, Japan, and [c]Tama Health Management Center, Tachikawa, Tokyo 190, Japan

A high-sensitivity HARPICON™ camera was developed for medical X-ray imaging using a fluorescent screen. It is an avalanche-multiplication-type image pick-up tube and is 32 times more sensitive than conventional tubes. The camera also has a wider dynamic range than conventional medical-imaging cameras because a maximum output signal current of 2.3 μA is obtained and, in high-illumination-intensity regions, photocurrent is not proportional to illumination intensity. The fluorescent screen is an intensifying screen of the type used for radiographic screen–film combinations in medical examination. An X-ray image on the screen is focused on the photoconductive layer of the pick-up tube using a coupling lens with $f/0.65$. Experiments were performed using monochromatized X-rays at the Photon Factory. An image of a spatial resolution test chart was taken in a 525 scanning-line mode of the camera. The chart pattern of 5 line-pairs mm^{-1} (spatial resolution of 100 μm) was observed at an X-ray input field of 50×50 mm. Real-time digital images of the heart of a 12 kg dog were obtained at a frame rate of 60 images s^{-1} after injection of a contrast medium into an artery. The images were stored in digital format at 512×480 pixels with 12 bits pixel^{-1}. High-spatial-resolution and high-contrast images of coronary arteries were obtained in aortography using X-rays with energy above that of the iodine K edge; the image quality was comparable with that of conventional selective coronary angiography.

Keywords: HARPICON camera; digital images; fluorescent screens; angiography.

1. Introduction

Real-time X-ray digital imaging systems using an X-ray image intensifier and a video camera have been widely used for medical imaging since the mid-1970s, in particular for digital subtraction angiography (Kruger & Riederer, 1984). Since then, spatial resolution has been improved by the use of X-ray image intensifiers and better video cameras. An X-ray image-intensifier tube consists of an input scintillator, an electron optical system and an output phosphor screen. In the tube an input X-ray image is converted into a minified output image with additional brightness gain. An X-ray image intensifier with a large output screen has high spatial resolution (Bates, 1980) because spatial resolution is decreased as the degree of minification increases (Kuhl, 1975). Recently, a high-spatial-resolution 2048 × 2048-pixel-matrix digital-radiography system has been introduced for gastrointestinal examination using an X-ray image intensifier with a large (60 mm diameter) output screen (Ogura et al., 1991). In this system, a limiting spatial resolution of 3.93 line-pairs mm^{-1} (127 μm resolution) was obtained with an 18 cm input field diameter of the

X-ray image intensifier and 2048 × 2048 digital samples. However, the value of 127 μm is larger than the effective pixel size of 95 μm because there are still limits on the spatial resolution of such X-ray image-intensifier video-camera systems.

High-resolution images can be obtained by using optical coupling via a high numerical aperture lens between a fluorescent screen and a high-sensitivity video camera without the X-ray image intensifier. A CCD (charge-coupled device) has been applied to small-input-field mammographic imaging, in a system in which the X-ray image on the screen is focused directly onto the CCD (Karellas, Harris, Liu, Davis & D'Orsi, 1992). Since only a small number of light photons emitted from the fluorescent screen are captured by the CCD, it is necessary, in this system, to operate the CCD at low temperatures and with long pixel-data readout times in order to achieve high-sensitivity imaging. In place of an optical lens, demagnifying tapered fibre-optic bundle coupling has been used for high optical coupling efficiency (Lowrance, Cope, Herron, Gur & Daxon, 1990; Roehrig, Fajardo, Yu & Schempp, 1994). Although these CCD systems are suitable for taking a high-resolution single image, they need higher sensitivity for high-speed real-time imaging. For example, to apply

---

† Present address: Musashino Division, Hitachi Device Engineering Company Ltd, Kokubunji, Tokyo 185, Japan.

the system to coronary angiography, proximity-type light-image intensifiers have been combined with tapered fibre-optic bundles for the CCD imaging system (Roehrig *et al.*, 1989).

A low-noise amplification process that does not use the X-ray image intensifier is required in video-camera fluorescent-screen optical-lens coupling systems for high-speed real-time imaging. Pick-up-tube camera systems have been investigated, using image-orthicon and image-isocon tubes, since the 1950s (Holmes & Wright, 1962; Sklensky & Buchanan, 1980). Both types of camera are return-beam pick-up-tube cameras. A visible image focused on a photocathode in the tube by an optical lens is transformed into photoelectrons. Then, the photoemissive electrons are accelerated to a storage-membrane target resulting in the first signal amplification. Finally, the input image is transformed into charge distribution on the target. A scanning electron beam interacts with the charged target to discharge it. Then, the beam returns backwards and is amplified for the second time by an electron multiplier to produce a video signal output (Nelson, Barbaric, Gomes, Moler & Deckard, 1982).

On the other hand, the HARPICON camera is a photoconductive target-type pick-up tube (Tanioka *et al.*, 1988; Takasaki *et al.*, 1988) and has been used for high-definition television (HDTV). For applications of the tube to the medical field, we developed a medical-imaging HARPICON camera with a sensitivity 32 times higher than conventional cameras. The camera also has an electron-beam current about ten times higher than conventional pick-up-tube cameras for a wide dynamic range, and has a high spatial resolution of 1050 video lines. A brief description of our camera has been presented elsewhere (Umetani, Kajiyama, Ueda, Takasaki & Yokouchi, 1994). Details of camera characteristics and an angiography system using monochromatized X-rays will be presented here. Since iodine is used as the contrast agent for angiography, high-contrast images of blood vessels are obtained by using monochromatized X-rays that have an energy just above the *K* edge of iodine. Application of our system suggests that a combination of the real-time high-spatial-resolution imaging system and monochromatized X-rays can be effective for the imaging of coronary arteries in aortography, which is less invasive than conventional selective coronary angiography.

2. Methods

2.1. *The HARPICON camera*

Imaging systems for real-time digital angiography need to have high frame rates and high image-acquisition speeds to avoid motion blurring, high spatial resolution, as well as high signal-to-noise ratios, to make thin vessels visible, and wide dynamic range to avoid signal saturation. To provide these features, television-camera tubes such as the SATICON™ and the PLUMBICON® have been improved for medical X-ray imaging (Kamiya *et al.*, 1986; Murphy, Bitler, Lybrook, Stevener & Broemmelsiek, 1994).

However, these conventional tubes have had to be used in combination with X-ray image intensifiers owing to low sensitivity. For low-noise and high-sensitivity imaging, a pick-up tube has to provide internal amplification processing.

The HARPICON camera is an image pick-up tube with an amorphous selenium (a-Se) photoconductive target and is characterized by its internal amplification process, which uses the avalanche phenomenon in a photoconductive layer. Fig. 1 shows an outline of the structure of the HARPICON camera. In the a-Se photoconductive layer, stable avalanche multiplication of photo-generated carriers occurs under a strong electric field (as high as 10^6 V cm^{-1}, *i.e.* about an order of magnitude higher than conventional tubes). Each incident light photon produces one electron–hole pair. The primary carriers contributing to the photocurrent are assumed to be holes that are accelerated towards the beam-scanning side of the photoconductive layer. Since these accelerated carriers collide with atoms to generate multiple new electron–hole pairs, a large number of carriers contribute to the output-signal current of the tube.

The multiplication factor, *M*, can be calculated using the following expression (Sze, 1981):

$$M = \frac{(\beta - \alpha) \exp[(\beta - \alpha)d]}{\beta - \alpha \exp[(\beta - \alpha)d]}, \qquad (1)$$

where *d* is the thickness of the a-Se layer and α and β denote the electron and hole impact-ionization rates, respectively. These rates are as follows (Tsuji *et al.*, 1991):

$$\alpha = 3.8 \times 10^7 \exp(-1.5 \times 10^7/E) \quad (\text{cm}^{-1}), \qquad (2)$$

$$\beta = 1.7 \times 10^7 \exp(-9.3 \times 10^6/E) \quad (\text{cm}^{-1}), \qquad (3)$$

where *E* is the strength of the electric field (V cm^{-1}).
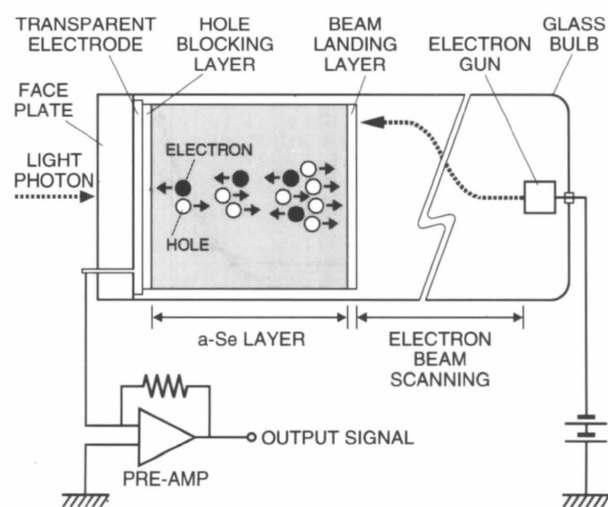

Figure 1
An outline of HARPICON's structure. After avalanche multiplication, electric charges stored on the beam-scanning side of the a-Se are read out by a scanning electron beam to produce output-signal current.

According to (1), a larger multiplication factor can be obtained by using a thicker photoconductive layer and/or by increasing the electric field.

Fig. 2 shows the dependence of both measured and calculated multiplication factors on the voltage applied to the photoconductive layer (target voltage). Measured values were obtained under the camera-operation conditions shown in Table 1 where the 525 scanning-line mode was selected, and under low illumination intensity of green light that produced the tube output-signal current of 0.3 μA at the target voltage of 461 V. The tube has a multiplication factor of 32 at 461 V and 1 at 340 V.

Calculations based on (1)–(3) and on the parameters of an a-Se layer thickness of 4 μm and target voltage of 483 V give a multiplication factor of 32. These expressions assume that the photoconductive layer consists of pure amorphous selenium. In Fig. 2 the solid line shows that the avalanche multiplication occurs at target voltages of more than 300 V.

The difference between the measured and calculated values in the avalanche-multiplication region is caused by the doping material used in the a-Se. The photoconductive selenium layer was doped with arsenic to prevent crystallization of amorphous selenium at high temperatures. In the doped photoconductive layer, the electric field is not uniform because of space charge caused by trapped electrons. Calculated values based on the non-uniform electric field will be able to fit the measured values in the avalanche-multiplication region.

Moreover, the measured values show no plateau region (where the multiplication factor is unity) at target voltages of less than 340 V because of recombination of photo-generated charges in the low-electric-field region. Calcu-

Table 1

Specifications of the HARPICON camera developed for the use of X-ray medical imaging.

The maximum signal and beam currents are much higher than those of conventional television-camera tubes.

Tube type	Magnetic focusing and electrostatic deflection
Tube diameter	1 in
Target thickness	4 μm
Target voltage	461 V
Multiplication	32
Electron gun	Barium-impregnated cathode and diode type
Beam current	2.5 μA
Signal current	2.3 μA (maximum)
Scanning area	12.5 × 12.5 mm
Scanning mode	Progressive (non-interlaced)
Scanning lines	1050 lines/15 Hz and 525 lines/60 Hz

lated values based on charge recombinations will also be able to fit the measured values in this region.

Fluctuation in the multiplication factor around the mean value results in generation of noise photocurrent. The signal-to-noise ratio is decreased by such excess noise in the case of an avalanche photodiode. However, the HARPICON camera has no excess noise because of the charge-storage operation of the tube. The stored charge suppresses the electric field caused by the target voltage. Since the avalanche-multiplication factor depends strongly on the electric field, the rate of increase of the stored signal charge varies according to the amount of previously stored signal charge on the electron-beam side of the a-Se layer. Each avalanche multiplication is not independent of others, depending instead on the history of past multiplications. This dependence suppresses fluctuations in the multiplication (Tsuji et al., 1991).

The photoelectric conversion characteristic is expressed by the γ value and the signal current (I_s) is given as follows:

$$I_s \propto L^\gamma. \tag{4}$$

where L is the intensity of incident light. In conventional pick-up tubes, the γ value is unity and characteristics respond linearly. However, in the HARPICON camera, the γ value is smaller than unity in the high-light-intensity region. Photoelectric conversion characteristics were measured at target voltages of 461 and 340 V, corresponding to the avalanche-multiplication and non-multiplication modes, respectively. The characteristics are shown in Fig. 3. The HARPICON camera in the non-multiplication mode has the γ value of unity in the high-light-intensity region and has the same characteristic with conventional tubes. In the avalanche-multiplication mode, the γ value decreases in the high-light-intensity region corresponding to signal-current values of more than 0.3 μA because of the decreasing multiplication factor.

Fig. 4 shows the dependence of the multiplication factor on the target voltage at two light-intensity conditions. The black circles are the same measured values as those in Fig. 2 and were obtained at the low-light-intensity
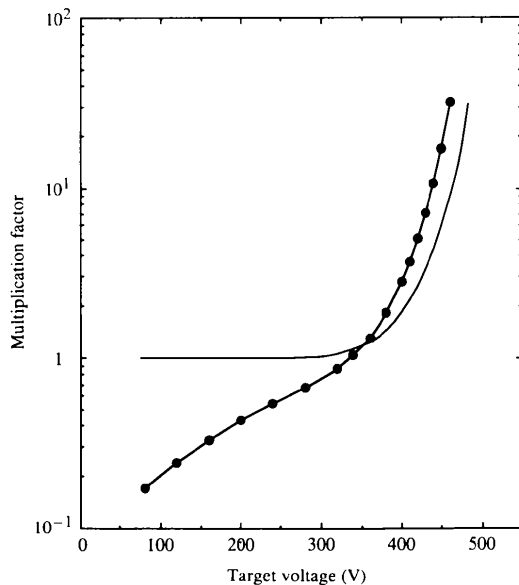

Figure 2

HARPICON's multiplication-factor dependence on target voltages. Black circles are measured values, where the data point of 32 times multiplication at 461 V has a signal current of 0.3 μA because of low illumination intensity. The solid line shows the values calculated using expressions (1)–(3).

condition that produced 0.3 µA signal current at the target voltage of 461 V. Data values shown by the white circles were measured at a *ca* 12 times higher light-intensity condition than that of the 0.3 µA output current, and the high light intensity produced a 2.2 µA signal current at 461 V. Compared with the 32 times multiplication at the low-light-intensity condition (0.3 µA signal current), the multiplication factor at the high-light-intensity condition
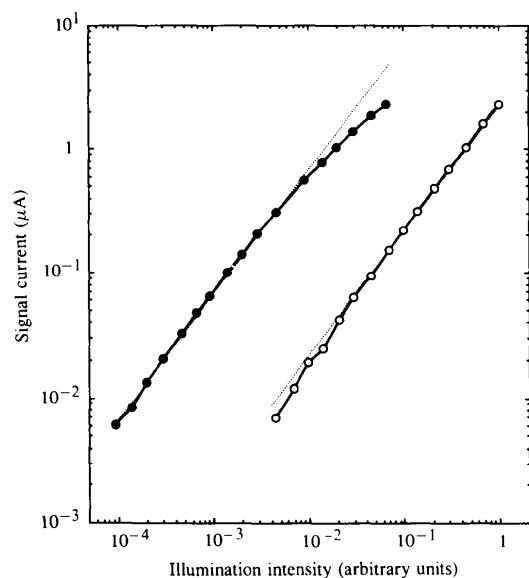

Figure 3
Photoelectric conversion characteristics measured at target voltages of 461 and 340 V corresponding to the avalanche-multiplication and non-multiplication modes, shown by black and white circles, respectively. The dotted straight lines show the values when $\gamma = 1$.
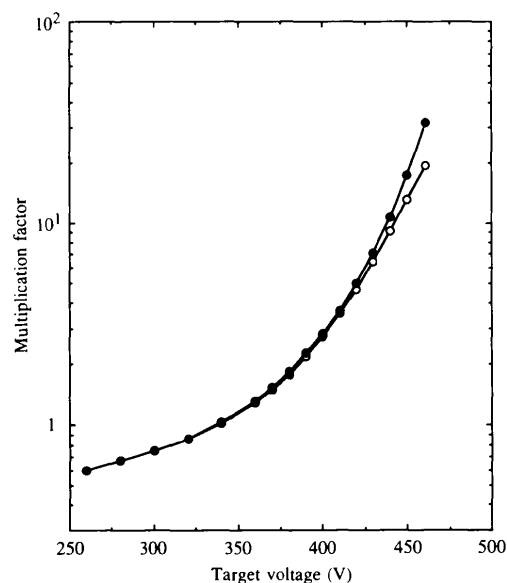

Figure 4
Multiplication-factor dependence on the target voltage at two illumination-intensity conditions. Black circles are the same values as those in Fig. 2. Data values shown by white circles were measured in a high-illumination-intensity condition, producing 2.2 µA signal current at 461 V.

(2.2 µA signal current) is 19.4 at 461 V. This is because the large amount of stored signal charge on the beam-scanning side of the a-Se layer, caused by the high-intensity incident light, decreases the electric field and thus the multiplication factor.

In the avalanche-multiplication mode, the γ value decreases in the high-light-intensity region owing to a decreasing multiplication factor. Low γ values can make dynamic ranges wider, and in Fig. 3 the camera has a dynamic range that is about three times wider in the avalanche-multiplication mode than in the non-multiplication mode.

Since the increased maximum signal current further expands the dynamic range, tubes for medical-imaging cameras have higher output signal currents than those of conventional television camera tubes to avoid image-quality degradation caused by signal saturation. Although the HARPICON tube can be operated at a beam current of up to 6 µA, more reasonable values of maximum beam and signal current were used because high beam current makes the dynamic range wide but makes the spatial resolution low. However, the selected 2.3 µA signal current and 2.5 µA beam current are much higher than conventional television-tube values of 0.3–0.6 µA each.

2.2. Imaging system

Medical X-ray imaging using synchrotron radiation for dual-energy iodine K-edge transvenous coronary angiography has been under investigation since the end of the 1970s (Thomlinson, 1992). Line-scanning systems with dual X-ray beams have been developed and improved for human clinical studies by American and German groups (Thompson *et al.*, 1994; Dix *et al.*, 1992). On the other hand, two-dimensional imaging systems using an X-ray image intensifier have been employed for real-time imaging in Japan (Fukagawa *et al.*, 1989; Umetani *et al.*, 1991; Takeda *et al.*, 1994). In the dual-energy method, pairs of images at energies higher and lower than the iodine K edge are taken and are used to produce subtraction images. Since iodine has a jump in X-ray absorption coefficient at the K-edge energy but body structures have no jump, organic structures outside of the circulatory system are eliminated by this subtraction operation, improving the sensitivity only to circulatory system structures, which contain a diluted iodine contrast material that has been injected venously.

On the other hand, a single-energy approach has been investigated for conventional angiography. Monochromatized X-rays with 33.3 keV energy (*i.e.* just above the iodine K-edge energy) are strongly absorbed by the iodine contrast material used for angiography (Hyodo, Nishimura & Ando, 1991). The conventional transvenous angiography method using monochromatized X-rays allows high-sensitivity images of the coronary arteries to be taken opacified with the contrast material (Takeda *et al.*, 1995). Furthermore, with the intra-arterial injection approach and 33.3 keV energy X-rays, images of arteries with very small diameters (less than 100 µm) can be obtained (Mori *et al.*, 1994).

Experiments in intra-arterial injection angiography with the single-energy approach were performed at the Photon Factory in Tsukuba, where the X-ray imaging system was placed at beamline BL-14C (Umetani *et al.*, 1993), see Fig. 5. BL-14 is a superconducting vertical wiggler beamline operated at a field strength of 5 T which produces a vertically oriented sheet-shaped beam. The height of the beam is restricted to 38 mm by a vertical aperture and the width is adjusted to 7 mm by an X-ray slit. The synchrotron radiation beam is monochromatized and expanded horizontally by an asymmetrically cut silicon ⟨311⟩ crystal. The monochromatized X-rays have a rectangular cross section of 70 × 38 mm (width × height) used for imaging.

In Fig. 5, X-rays passing through an object are transformed into a visible image by a fluorescent screen, in this case an HR-4 screen (Fuji Medical Systems Co. Ltd, Japan), usually used as an X-ray screen–film system in medical examinations. This screen uses a gadolinium oxysulfide (Gd_2O_2S:Tb) phosphor, the peak light emission of which is centred at 550 nm. The thickness of the phosphor layer is 115 μm. The density of phosphor particles is 7.34 g cm^{-3} and the degree of packing of the phosphor layer is *ca* 60%. Images of dimensions 50 × 50 mm on the screen were read by a HARPICON camera with a lens. To couple the screen to the HARPICON tube, we applied a relay lens system that had been developed for the X-ray image-intensifier video-camera system (Ogura *et al.*, 1991) in which an image on the output screen of the X-ray image intensifier is focused onto the photoconductive layer of the camera tube. The lens has an aperture of *f*/0.65 and 4:1 demagnification factor. An image on the screen is focused onto an electron-beam scanning area of 12.5 × 12.5 mm on the HARPICON camera's photoconductive layer.

In our image-acquisition system, image signals from the camera are converted into digital format by an analogue-to-digital converter with 12-bit resolution and are stored in a frame memory with a total capacity of 144 Mbyte. The image-acquisition system takes 512 × 480-pixel and 1024 × 960-pixel digital images corresponding to the camera's 525 and 1050 scanning-line modes at acquisition rates

of 60 and 15 images s^{-1}, respectively. The total numbers of stored images are 384 and 96 with formats of 512 × 480 and 1024 × 960 pixels, respectively. Images in the frame memory are finally archived in a long-term storage device, in this case a 10 Gbyte digital video-cassette recorder. After acquisition, images are transferred to a workstation (Hewlett-Packard HP715/33) by a DR11W interface and image-processing operations are performed.

In video-camera fluorescent-screen lens-coupling systems, very small proportions of the light photons emitted by the fluorescent screen after X-ray absorption are passed to the video camera because of the low optical-coupling efficiency of the lens. The efficiency characteristics of such image detectors are defined by the number of photo-generated electron–hole pairs per one X-ray photon absorption (Karellas *et al.*, 1992). The number of charge pairs, N, can be calculated as the product of the efficiencies of all preceding stages:

$$N = E_X \eta_P \omega_F \omega_L \eta_{HARP}/E_L,   (5)$$

where E_X is the incident X-ray-photon energy (33 300 eV), η_P is the screen's X-ray-to-light-photon energy-conversion efficiency (0.15), E_L is the energy of light photons of 550 nm wavelength (2.25 eV), ω_F is the ratio of photons passed to the surface from inside of the screen (0.5), ω_L is the optical-lens coupling efficiency and η_{HARP} is the generation efficiency of photo-charge electron–hole pairs in the a-Se layer per one incident light photon (0.5). The values in the parentheses are the parameters of the present system; the η_P value was obtained from the manufacturer (Kasei Optonix Ltd, Japan). The optical-lens coupling efficiency (Liu, Karellas, Harris & D'Orsi, 1994) is calculated by

$$\omega_L = T/[1 + 4f^2(m + 1)^2],   (6)$$

where T is the transmission factor of the lens (0.9), f is the *f*-number (0.65) and m is the demagnification factor (4.0). From (5) and (6), we can estimate that the number of photo-
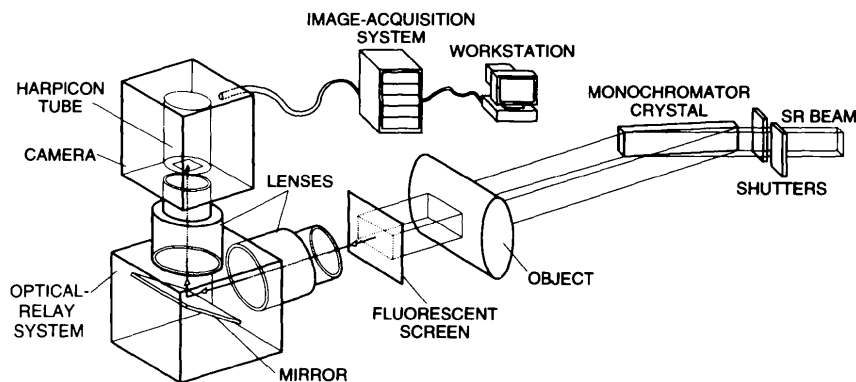

Figure 5
Schematic drawing of the imaging system. A 33.3 keV X-ray image is transformed into a visible image by a fluorescent screen. The 50 × 50 mm images on the screen are read by the HARPICON camera with 1050 or 525 scanning lines *via* an optical-relay system. After analogue-to-digital conversion, images are stored in an image-acquisition system.

generated charge pairs N will be ~11.5. In the present system, 11.5 electron–hole charge-pairs are produced in the a-Se layer after absorption of one 33.3 keV X-ray photon by the fluorescent screen, and the number of holes is multiplied 32 times by avalanche multiplication to produce the output-signal current.

Assuming Poisson statistics, the signal-to-noise ratio (SNR) of the lens-coupled imaging chain is given in (7) (Liu *et al.*, 1994):

$$SNR = N_X^{1/2}/[1 + (1/N)]^{1/2}. \qquad (7)$$

where N_X is the number of X-ray photons absorbed by the screen per pixel. When $N = 11.5$, $SNR = 0.96 N_X^{1/2} \simeq N_X^{1/2}$. The N value of 11.5 shows that the SNR of the system is due predominantly not to the optical-lens coupling efficiency from the screen to the camera but to X-ray quantum noise. This means that our system is an X-ray quantum-noise-limited imaging system, so an excess X-ray dose is not required for imaging.

3. Experiment and results

3.1. Spatial resolution

The spatial resolution of the HARPICON camera was measured by taking an image of an optical test chart *via* a photographic camera lens. In the 1050 scanning-line mode, the peak-to-peak square-wave amplitude response is 50% for the chart pattern corresponding to 800 TV lines at the centre of the photoconductive target. The camera has the capability of taking a sharp 1024 × 960-pixel format image.

An X-ray spatial-resolution chart was placed on the detector input plane to examine the resolution of the image detector. An X-ray image of the chart taken in the 1050 scanning-line mode is shown in Fig. 6. The chart pattern at the bottom of the image shows slight 50 μm-width stripes when the picture is viewed at a grazing angle. The limiting spatial resolution of this system is $\simeq$ 10 line-pairs mm^{-1}. Since the input-field size is 50 × 50 mm and images were digitized at 1024 × 960 pixels, the single-pixel size on the screen surface is ~50 μm. Spatial resolution of 50 μm is the same as that defined by the pixel size.

For high-speed real-time imaging, the 525 scanning-line mode is selected to take the 512 × 480-pixel image in 16.7 ms because it takes 66.7 ms to obtain each 1024 × 960-pixel image. An image of another X-ray chart was obtained in 512 × 480-pixel format and is shown in Fig. 7. Since the spatial resolution of the system is defined by the pixel size, the limiting spatial resolution is 5 line-pairs mm^{-1} and the chart pattern of 100 μm-width stripes is shown clearly at the bottom of the chart image.

3.2. Coronary angiography

In vivo imaging of intra-arterial injection angiography with the single-energy approach was performed on a dog at the BL-14C. The X-ray energy was adjusted to 33.3 keV *via* the monochromator. When the storage ring was operated at 2.5 GeV and the beam current was 290–330 mA, the X-ray flux was ~8.2 × 10^8 photons mm^{-2} s^{-1} on the object surface, measured after the X-rays had passed through a 0.5 mm-thick aluminium filter used to remove very low energy X-ray components. Real-time angiographic images were taken in the 525 scanning-line mode at an acquisition rate of 60 images s^{-1}. Each image was obtained in 16.7 ms with a dose of ~0.87 mSv.
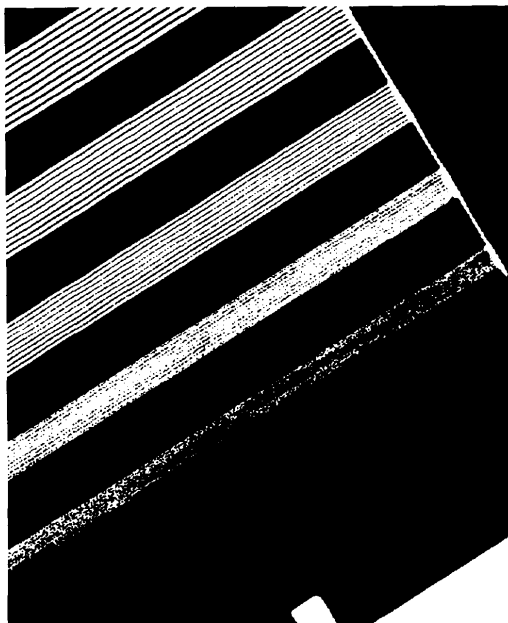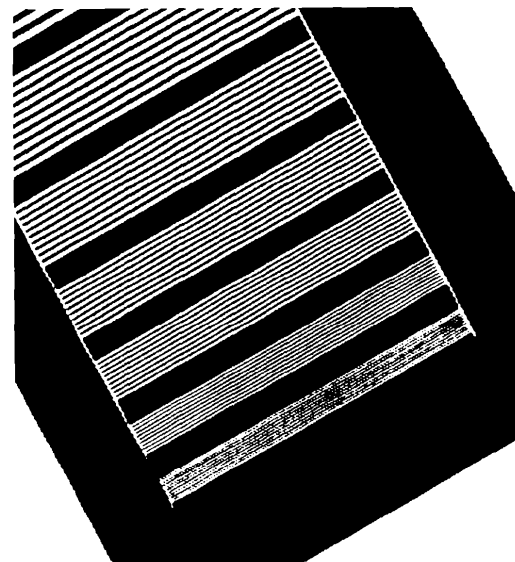

Figure 6
X-ray image of the spatial resolution chart taken in the 1050 scanning-line mode. The spatial frequencies are, from bottom to top, 10, 8, 6, 5 and 4 line-pairs mm^{-1}.

Figure 7
Spatial resolution chart image taken in the 525 scanning-line mode. The spatial frequencies are, from bottom to top, 5, 4, 3, 2.5, 2 and 1.5 line-pairs mm^{-1}.

The dog, weighing 12 kg, was anesthetized with Nembutal[R]. A catheter was inserted into the aorta *via* the right femoral artery and the catheter tip was placed near the aortic valve. Another catheter was inserted into the pulmonary artery *via* the superior vena cava and the right ventricle. Initially, the canine coronary arteries were imaged after contrast material injection to the pulmonary artery. 12 ml of iodine contrast material (Iomeron[R] 350) was injected at a rate of $12\,\mathrm{ml\,s^{-1}}$ by an M-800C injector (Nemoto Kyorindo Co. Ltd, Japan). Later aortographic images were obtained after 10 ml contrast material injection to the aorta at a rate of $12\,\mathrm{ml\,s^{-1}}$ and were taken in the same imaging direction as that of the pulmonary artery injection.

Figs. 8(*a*) and 8(*b*) show the image of the pulmonary artery injection and the aortographic image taken in the same lateral view at 4.7 and 1.1 s after the start of injection, respectively. The actual size of the images is 50 mm-width and 38 mm-height and is restricted by the cross section of the X-ray beam and the input field size of the image detector.

Before these experiments, images of transvenous coronary angiography had been obtained at beamline BLNE-5A of the TRISTAN accumulation ring in Tsukuba by contrast material injection to the inferior vena cava using 33.3 keV X-rays, above the iodine *K*-edge energy (Takeda *et al.*, 1995). Compared with the images of Takeda *et al.*, a higher contrast image of the left anterior descending artery shown in Fig. 8(*a*) was obtained by injection directly to the pulmonary artery. However, the aortographic image in Fig. 8(*b*) shows arteries of much higher contrast and is sufficient for medical examination and diagnosis. In particular, the obtuse marginal branch of the left circumflex artery is shown in Fig. 8(*b*) but it is not shown in Fig. 8(*a*) because of low image contrast and overlap with the left ventricle. The inside diameter of the left anterior descending artery is less than 2 mm because the outside diameter of the catheter is ~2.2 mm.

Figure 8
Images of the dog's heart taken by (*a*) pulmonary artery injection, and (*b*) injection to the aorta in the same lateral view. The images show the left anterior descending artery (LAD), the left circumflex artery (LCX), the obtuse marginal branch (OMB), the right coronary artery (RCA), the left ventricle (LV), the aorta (AO) and the catheter for the pulmonary artery injection (CA).
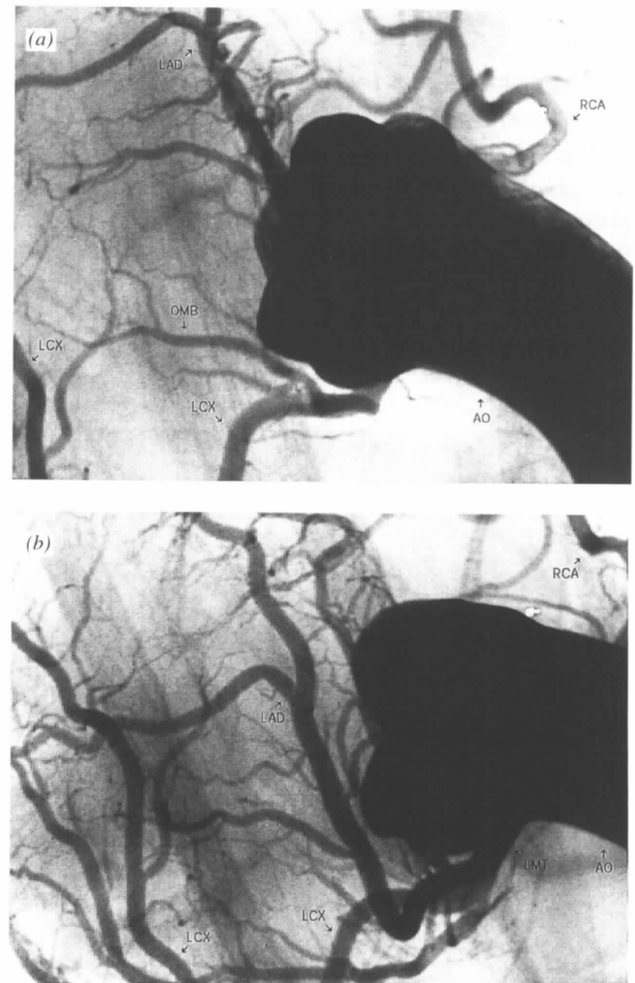

Figure 9
Aortographic images of the 12 kg dog taken in different imaging directions. The images show the left anterior descending artery (LAD), the left circumflex artery (LCX), the obtuse marginal branch (OMB), the left main trunk (LMT), the right coronary artery (RCA) and the aorta (AO).

After the catheter placed in the pulmonary artery was removed, aortographic images of the same dog were taken in the two imaging directions. The images in Fig. 9 were obtained 1.2 s after the start of injection. 12 ml of iodinated contrast agent was injected at a rate of 9 ml s⁻¹ for each image. Fig. 9(*a*) shows three coronary arteries with image quality comparable with that of conventional selective coronary angiography. If the image size is about two times larger than that in Fig. 9, all structures of the three coronary arteries will be imaged by the single injection. Furthermore, an aortographic approach is a safer method than selective coronary angiography, in which the catheter tip is inserted into each coronary artery.

The image in Fig. 9(*b*) was obtained after a 30° rotation of the dog's body from the position in Fig. 9(*a*). The image clearly shows the left main trunk and division into the left anterior descending artery and the left circumflex artery.

The imaging system using 33.3 keV X-rays takes real-time high-quality images of coronary arteries but requires a higher radiation dose than that of conventional angiography systems using an X-ray tube. For practical diagnostic imaging under the maximum tolerable dose, the reasonable number of images is 30–40 in total. For example, an imaging cycle is 10 images s⁻¹ and an imaging time is 3–4 s.

The experiment was approved by the Medical Committee for the Use of Animals in Research of the University of Tsukuba, and conformed to the guidelines of the American Physiological Society.

4. Future system

We proposed an energy-selective detector for iodine *K*-edge dual-energy imaging in §4.2 of Umetani *et al.* (1993). There, a combination of a light-image intensifier and a conventional video camera recorded images on the fluorescent screen. By using the HARPICON camera in that system, images on the screen can be obtained directly without the light-image intensifier.

The new system is shown in Fig. 10. An NaI(Tl) scintillator is used which absorbs more higher-energy X-ray components than iodine *K*-edge energy X-rays when the

monochromatized X-ray energy is adjusted to centre on the iodine *K* edge. A high-energy image is produced on the first of the NaI(Tl) scintillator-plate screens, and is directly detected by the HARPICON camera. Low-energy X-rays passing through the first screen produce a low-energy image on the second screen, and are detected by the separate HARPICON camera. Subtraction of the two images decreases the contrast of non-vascular body structures but enhances the contrast of the iodine-opacified vascular system. The HARPICON–fluorescent screen system is suitable for the energy-selective detector.

5. Concluding remarks

A HARPICON camera with 32 times higher sensitivity than that of conventional pick-up-tube cameras and with 2.5 μA beam current and 2.3 μA signal current was developed for X-ray medical imaging using a fluorescent-screen lens-coupling approach. The imaging system achieved the high spatial resolution of 10 and 5 line-pairs mm⁻¹ (50 and 100 μm resolution) with a 50 × 50 mm input-field size in the 1050 and 525 scanning-line modes, respectively. In particular, each image in the 525 scanning-line mode can be taken in 16.7 ms at a rate of 60 images s⁻¹.

Since very small proportions of the light photons emitted by the fluorescent screen after X-ray absorption are passed to the video camera, high optical-coupling efficiency of the lens is important. To couple the screen to the HARPICON camera, we applied a relay lens system with an aperture of *f*/0.65. The number of photo-generated charge pairs is ∼11.5 after an X-ray photon absorption. This means that our system is an X-ray quantum-noise-limited imaging system, so an excess X-ray dose is not required for imaging.

Monochromatized X-rays of 33.3 keV, *i.e.* just above the iodine *K*-edge energy, can produce high-sensitivity images in angiography with iodine-contrast-material injection. Preliminary medical-imaging studies of a high-spatial-resolution system were performed using intra-arterial injection angiography in a dog.

In aortographic imaging with a catheter tip inserted into the aorta and placed near the aortic valve, the left anterior
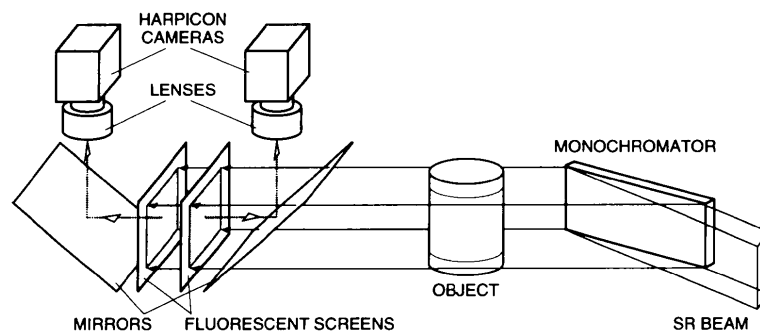

Figure 10
Schematic drawing of the energy-selective detector. The high-energy image is produced on the first screen, which consists of an NaI(Tl) scintillator and is read by the HARPICON camera. Low-energy X-rays passing through the first screen produce the low-energy image on the second screen.

descending artery, the left circumflex artery and the right coronary artery were all visualized in a single injection of the contrast material with image quality comparable with that of conventional selective coronary angiography. Furthermore, the left main trunk and division into the left anterior descending artery and the left circumflex artery were imaged clearly. This type of aortographic approach to coronary arterial diagnosis is less invasive than conventional selective coronary angiography, in which the catheter tip is inserted into each coronary artery.

The imaging system using X-rays above the iodine K-edge energy takes real-time high-quality images but requires a high radiation dose. For diagnostic imaging under a tolerable dose, the reasonable number of images is 30–40 in total.

References

Bates, C. W. Jr (1980). Real-Time Radiologic Imaging: Medical and Industrial Applications, edited by D. A. Garrett & D. A. Bracher, pp. 45–65. Philadelphia: American Society for Testing and Materials.

Dix, W.-R., Engelke, K., Graeff, W., Hamm, C., Heuer, J., Kaempf, B., Kupper, W., Lohmann, M., Reime, B. & Reumann, R. (1992). Nucl. Instrum. Methods, A314, 307–315.

Fukagawa, H., Noda, C., Suzuki, Y., Hasegawa, S., Ando, M., Hyodo, K., Nishimura, K., Akisada, M., Takenaka, E., Hosaka, R. & Toyofuku, F. (1989). Rev. Sci. Instrum. 60, 2268–2271.

Holmes, R. B. & Wright, D. J. (1962). Radiology, 79, 740–751.

Hyodo, K., Nishimura, K. & Ando, M. (1991). Handbook on Synchrotron Radiation, Vol. 4, edited by S. Ebashi, M. Koch & E. Rubenstein, ch. 2. Amsterdam: Elsevier Science.

Kamiya, M., Takahashi, F., Tsuneoka, M., Hayashi, T., Yokouchi, H. & Takahashi, M. (1986). SPIE Medicine XIV/PACS IV, 626, 366–372.

Karellas, A., Harris, L. J., Liu, H., Davis, M. A. & D'Orsi, C. J. (1992). Med. Phys. 19, 1015–1023.

Kruger, R. A. & Riederer, S. J. (1984). Basic Concepts of Digital Subtraction Angiography. Boston: G. K. Hall Medical Publishers.

Kuhl, W. (1975). SPIE Medical X-ray, 56, 80–84.

Liu, H., Karellas, A., Harris, L. J. & D'Orsi, C. J. (1994). Med. Phys. 21, 1193–1195.

Lowrance, J. L., Cope, A. D., Herron, J. M., Gur, D. & Daxon, E. G. (1990). SPIE Charge-Coupled Devices and Solid State Optical Sensors, 1242, 59–65.

Mori, H., Hyodo, K., Tobita, K., Chujo, M., Shinozaki, Y., Sugishita, Y. & Ando, M. (1994). Circulation, 89, 863–871.

Murphy, G., Bitler, W., Lybrook, J., Stevener, T. & Broemmelsiek, M. (1994). SPIE Physics of Medical Imaging, 2163, 333–342.

Nelson, R. S., Barbaric, Z. L., Gomes, A. S., Moler, C. L. & Deckard, M. E. (1982). Med. Phys. 9, 777–783.

Ogura, T., Masuda, Y., Fujita, H., Inoue, N., Yonekura, F., Miyagi, Y., Takatsu, K., Akahira, K., Tsuruta, S., Kamiya, M., Takahashi, F., Oda, K., Ikeda, S. & Koike, K. (1991). SPIE Medical Imaging V: Imaging Physics, 1443, 153–159.

Roehrig, H., Dallas, W., Lamoreaux, R., McNeill, K., Ovitt, T. W. & Vercillo, R. (1989). SPIE Medical Imaging III: Image Formation, 1090, 377–388.

Roehrig, H., Fajardo, L. L., Yu, T. & Schempp, W. S. (1994). SPIE Physics of Medical Imaging, 2163, 320–332.

Sklensky, A. F. & Buchanan, R. A. (1980). Real-Time Radiologic Imaging: Medical and Industrial Applications, edited by D. A. Garrett & D. A. Bracher, pp. 315–329. Philadelphia: American Society for Testing and Materials.

Sze, S. M. (1981). Physics of Semiconductor Devices, 2nd ed., ch. 1. New York: John Wiley.

Takasaki, Y., Tsuji, K., Hirai, T., Maruyama, E., Tanioka, K., Yamazaki, J., Shidara, K. & Taketoshi, K. (1988). Mater. Res. Soc. Symp. Proc. 118, 387–397.

Takeda, T., Itai, Y., Wu, J., Ohtsuka, S., Hyodo, K., Ando, M., Nishimura, K., Hasegawa, S., Akatsuka, T. & Akisada, M. (1995). Acad. Radiol. 2, 602–608.

Takeda, T., Itai, Y., Yoshioka, H., Umetani, K., Ueda, K. & Akisada, M. (1994). Med. Biol. Eng. Comput. 32, 462–468.

Tanioka, K., Yamazaki, J., Shidara, K., Taketoshi, K., Kawamura, T., Hirai, T. & Takasaki, Y. (1988). Adv. Electron. Electron Phys. 74, 379–387.

Thomlinson, W. (1992). Nucl. Instrum. Methods, A319, 295–304.

Thompson, A. C., Lavender, W. M., Chapman, D., Gmur, N., Thomlinson, W., Rosso, V., Schulze, C., Rubenstein, E., Giacomini, J. C., Gordon, H. J. & Dervan, P. J. (1994). Nucl. Instrum. Methods, A347, 545–552.

Tsuji, K., Ohshima, T., Hirai, T., Gotoh, N., Tanioka, K. & Shidara, K. (1991). Mater. Res. Soc. Symp. Proc. 219, 507–518.

Umetani, K., Kajiyama, T., Ueda, K., Takasaki, Y. & Yokouchi, H. (1994). SPIE Physics of Medical Imaging, 2163, 361–365.

Umetani, K., Ueda, K., Takeda, T., Akisada, M., Nakajima, T. & Anno, I. (1991). Nucl. Instrum. Methods, A301, 579–588.

Umetani, K., Ueda, K., Takeda, T., Itai, Y., Akisada, M. & Nakajima, T. (1993). Nucl. Instrum. Methods, A335, 569–579.